Comparison of different proximity potentials for asymmetric colliding nuclei

Ishwar Dutt and Rajeev K. Puri[*]

Department of Physics, Panjab University, Chandigarh 160014, India
(Received 3 April 2010; published 21 June 2010)

Using the different versions of phenomenological proximity potential as well as other parametrizations within the proximity concept, we perform a detailed comparative study of fusion barriers for asymmetric colliding nuclei with asymmetry parameter as high as 0.23. In all, 12 different proximity potentials are robust against the experimental data of 60 reactions. Our detailed study reveals that the surface energy coefficient as well as radius of the colliding nuclei depend significantly on the asymmetry parameter. All models are able to explain the fusion barrier heights within ±10% on the average. The potentials due to Bass 80, AW 95, and Denisov DP explain nicely the fusion cross sections at above- as well as below-barrier energies.

I. INTRODUCTION

The fusion of colliding nuclei with neutron-rich/-deficient content and at the extreme of isospin plane has attracted a large number of studies in recent years [1–11]. This renewed interest is due to the availability of radioactive-ion beams that can produce nuclei at the extreme of isospin [1,10,11]. Further, this field has also been enriched with several new phenomena that put a stringent test on theoretical models derived to study the fusion phenomenon in heavy-ion reactions.

As is evident from the literature, no experiment can extract information about the fusion barriers directly. All experiments measure the fusion differential cross sections [1–3] and then with the help of theoretical model, one extracts the fusion barriers. Theoretical models are very helpful in understanding the nuclear interactions at a microscopic level. A vast number of theoretical models and potentials have become available in recent years that can explain one or the other features of fusion dynamics [12–26].

In the galaxy of different theoretical models, proximity potential [13] enjoys very popular status. This phenomenological potential is a benchmark and backbone for all microscopic/macroscopic fusion models. It is almost mandatory to compare the potential and parametrize it within the proximity concept for wider acceptability. In recent years, several refinements and modifications have been proposed over original proximity potential [14,15]. Further, with the passage of time, different versions of the same model are also available [12]. Many of these modifications are based on the isospin effects either through the surface energy coefficients or via nuclear radius. It would be of interest to test these potentials in the isospin plane and to see how these different potentials will perform when asymmetry in the neutron/proton content is very large.

Recently, we carried out a detailed comparative systematic study of different fusion models for symmetric colliding nuclei [12]. Here we plan to extend this study for those colliding nuclei that have larger neutron/proton content. In this study, we shall compare as many as 12 proximity

potentials with different versions. This will include four versions of proximity potential: three versions of potential due to Bass and Winther each and the latest potential due to Ngô and a modified version of the Denisov potential. Section II deals with formalism in detail, Sec. III contains the results, and a summary is presented in Sec. IV.

II. FORMALISM

In this section, we present the details of various proximity potentials used for the calculation of fusion barriers. When two surfaces approach each other within a distance of 2–3 fm, additional force due to the proximity of the surface is labeled as proximity potential. Various versions of these potentials take care of different aspects including the isospin dependence. In the following, we discuss each of them in detail.

A. Proximity 1977 (Prox 77)

The basis of proximity potential is the theorem that states that "the force between two gently curved surfaces in close proximity is proportional to the interaction potential per unit area between the two flat surfaces." According to the original version of proximity potential 1977 [13], the interaction potential $V_N(r)$ between two surfaces can be written as:

$$V_N(r) = 4\pi\gamma b\overline{R}\Phi\left(\frac{r - C_1 - C_2}{b}\right) \text{MeV}. \quad (1)$$

In this, the mean curvature radius, $\overline{R}$, has the form

$$\overline{R} = \frac{C_1 C_2}{C_1 + C_2}, \quad (2)$$

quite similar to the one used for reduced mass. Here

$$C_i = R_i\left[1 - \left(\frac{b}{R_i}\right)^2 + \cdots\cdots\right], \quad (3)$$

R_i, the effective sharp radius, reads as

$$R_i = 1.28A_i^{1/3} - 0.76 + 0.8A_i^{-1/3} \text{ fm} \quad (i = 1, 2). \quad (4)$$

In Eq. (1), $\Phi(\xi = \frac{r - C_1 - C_2}{b})$ is a universal function that depends on the separation between the surfaces of two colliding nuclei

---

*rkpuri@pu.ac.in; drrkpuri@gmail.com

only. As we see, both these factors do not depend on the isospin content. However, γ, the surface energy coefficient, depends on the neutron/proton excess as

$$\gamma = \gamma_0 \left[1 - k_s \left(\frac{N - Z}{N + Z} \right)^2 \right], \qquad (5)$$

where N and Z are the total number of neutrons and protons. In the present version, γ_0 and k_s were taken to be 0.9517 MeV/fm^2 and 1.7826, respectively. Note that for the symmetric colliding pair, i.e., $(N = Z)$, $\gamma = \gamma_0 = 0.9517$ MeV/fm^2. If the $\left(\frac{N-Z}{N+Z}\right)$ ratio is 0.5, γ reduces to 0.5276 MeV/fm^2. Defining asymmetry parameter $A_s = \left[\frac{N_1 + N_2 - (Z_1 + Z_2)}{N_1 + N_2 + (Z_1 + Z_2)} \right]$, one notices drastic reduction in the magnitude of the potential with asymmetry of the colliding pair. Interestingly, most of the modified proximity type potentials use different values of the parameter γ [14,15].

The universal function $\Phi(\xi)$ was parameterized with the following form:

$$\Phi(\xi) = \begin{cases} -\frac{1}{2}(\xi - 2.54)^2 - 0.0852(\xi - 2.54)^3, \\ \qquad \text{for } \xi \leqslant 1.2511, \\ -3.437 \exp(-\xi/0.75), \\ \qquad \text{for } \xi \geqslant 1.2511. \end{cases} \qquad (6)$$

The surface width b has been evaluated close to unity. Using the above form, one can calculate the nuclear part of the interaction potential $V_N(r)$. This model is referred to as Prox 77 and the corresponding potential as $V_N^{\text{Prox77}}(r)$.

B. Proximity 1988 (Prox 88)

Later on, using the more refined mass formula due to Möller and Nix [27], the value of coefficients γ_0 and k_s were modified yielding the values $= 1.2496$ MeV/fm^2 and 2.3, respectively. Reisdorf [14] labeled this modified version as "Proximity 1988." Note that this set of coefficients give stronger attraction compared to the above set. Even a more recent compilation by Möller and Nix [28] yields similar results. We labeled this potential Prox 88.

C. Proximity 2000 (Prox 00)

Recently, Myers and Świątecki [15] modified Eq. (1) by using up-to-date knowledge of nuclear radii and surface tension coefficients using their droplet model concept. The prime aim behind this attempt was to remove descripency of the order of 4% reported between the results of Prox 77 and experimental data [15]. Using the droplet model [29], matter radius C_i was calculated as

$$C_i = c_i + \frac{N_i}{A_i} t_i \quad (i = 1, 2), \qquad (7)$$

where c_i denotes the half-density radii of the charge distribution and t_i is the neutron skin of the nucleus. To calculate c_i, these authors [15] used two-parameter Fermi function values given in Ref. [30] and the remaining cases were handled with the help of parametrization of charge distribution described

below. The nuclear charge radius (denoted as R_{00} in Ref. [31]), is given by the relation:

$$\begin{aligned} R_{00i} &= \sqrt{\frac{5}{3}} \langle r^2 \rangle^{1/2} \\ &= 1.240 A_i^{1/3} \left\{ 1 + \frac{1.646}{A_i} - 0.191 \left(\frac{A_i - 2Z_i}{A_i} \right) \right\} \text{ fm} \\ &(i = 1, 2), \end{aligned} \qquad (8)$$

where $\langle r^2 \rangle$ represents the mean-square nuclear charge radius. According to Ref. [31], Eq. (8) was valid for the even-even nuclei with $8 \leqslant Z < 38$ only. For nuclei with $Z \geqslant 38$, the above equation was modified by Pomorski *et al.* [31] as

$$R_{00i} = 1.256 A_i^{1/3} \left\{ 1 - 0.202 \left(\frac{A_i - 2Z_i}{A_i} \right) \right\} \text{ fm}$$
$$(i = 1, 2). \qquad (9)$$

These expressions give good estimate of the measured mean-square nuclear charge radius $\langle r^2 \rangle$. In the present model, authors used only Eq. (8). The half-density radius, c_i, was obtained from the relation:

$$c_i = R_{00i} \left(1 - \frac{7}{2} \frac{b^2}{R_{00i}^2} - \frac{49}{8} \frac{b^4}{R_{00i}^4} + \cdots \cdots \right) \quad (i = 1, 2). \qquad (10)$$

Using the droplet model [29], neutron skin t_i reads as

$$t_i = \frac{3}{2} r_0 \left(\frac{J I_i - \frac{1}{12} c_1 Z_i A_i^{-1/3}}{Q + \frac{9}{4} J A_i^{-1/3}} \right) (i = 1, 2). \qquad (11)$$

Here r_0 is 1.14 fm, the value of nuclear symmetric energy coefficient $J = 32.65$ MeV, and $c_1 = 3e^2/5r_0 = 0.757895$ MeV. The neutron skin stiffness coefficient Q was taken to be 35.4 MeV. The nuclear surface energy coefficient γ in terms of neutron skin was given as

$$\gamma = \frac{1}{4\pi r_0^2} \left[18.63(\text{MeV}) - Q \frac{(t_1^2 + t_2^2)}{2 r_0^2} \right], \qquad (12)$$

where t_1 and t_2 were calculated using Eq. (11). The universal function $\Phi(\xi)$ was reported as

$$\Phi(\xi) = \begin{cases} -0.1353 + \sum\limits_{n=0}^{5} [c_n/(n+1)](2.5 - \xi)^{n+1}, \\ \qquad \text{for} \quad 0 < \xi \leqslant 2.5, \\ -0.09551 \exp[(2.75 - \xi)/0.7176], \\ \qquad \text{for} \quad \xi \geqslant 2.5. \end{cases} \qquad (13)$$

The values of different constants c_n were $c_0 = -0.1886$, $c_1 = -0.2628$, $c_2 = -0.15216$, $c_3 = -0.04562$, $c_4 = 0.069136$, and $c_5 = -0.011454$. For $\xi > 2.74$, the above exponential expression is the exact representation of the Thomas-Fermi extension of the proximity potential. This potential is labeled Prox 00.

D. Modified Proximity 2000 (Prox 00DP)

Recently, Royer and Rousseau [22] modified Eq. (8) with slightly different constants as

$$R_{00i} = 1.2332 A_i^{1/3} \left[1 + \frac{2.348443}{A_i} \right.$$
$$\left. - 0.151541 \left(\frac{A_i - 2Z_i}{A_i} \right) \right] \text{fm} \quad (i = 1, 2). \quad (14)$$

It is obtained by analyzing as many as 2027 masses with N, $Z \geqslant 8$ and a mass uncertainty $\leqslant 150$ keV. Further, the accuracy of the above formula is mainly improved by adding the Coulomb diffuseness correction or the charge exchange correction to the mass formulas [22]. We implement this radius in the proximity 2000 version instead of the form given in the proximity 2000. This new version of the proximity potential is labeled Prox 00DP [12].

E. Bass 1973 (Bass 73)

This model is based on the assumption of liquid-drop model [16]. Here change in the surface energy of two fragments due to their mutual separation is represented by exponential factor. By multiply with geometrical arguments, one can obtained the nuclear part of the interaction potential as

$$V_N(r)^{\text{Bass73}} = -\frac{d}{R_{12}} a_s A_1^{1/3} A_2^{1/3} \exp\left(-\frac{r - R_{12}}{d} \right) \text{MeV}, \quad (15)$$

with $R_{12} = r_0(A_1^{1/3} + A_2^{1/3})$, $d = 1.35$ fm, and $a_s = 17.0$ MeV. The cut-off distance R_{12} is chosen to yield saturation density in the overlap region and $r_o = 1.07$ fm corresponding half of the maximum density for individual nucleus. We labeled this potential Bass 73.

F. Bass 1977 (Bass 77)

In this model, nucleus-nucleus potential is derived from the information based on the experimental fusion cross sections by using the liquid drop model and general geometrical arguments. The nuclear part of the potential (for spherical nuclei with frozen densities) can be written as [17]

$$V_N(r)^{\text{Bass77}} = -4\pi\gamma \frac{R_1 R_2}{R_1 + R_2} f(r - R_1 - R_2)$$
$$= -\frac{R_1 R_2}{R_1 + R_2} \Phi(r - R_1 - R_2) \text{MeV}, \quad (16)$$

with

$$\frac{df}{ds} = -1, \quad \text{for} \quad s = 0. \quad (17)$$

Note that $f(s = r - R_1 - R_2)$ and $\Phi(s = r - R_1 - R_2)$ are the universal functions. Here radius R_i is written as

$$R_i = 1.16 A_i^{1/3} - 1.39 A_i^{-1/3} \text{ fm} \quad (i = 1, 2). \quad (18)$$

The form of the universal function $\Phi(s)$ reads as

$$\Phi(s) = \left[A \exp\left(\frac{s}{d_1} \right) + B \exp\left(\frac{s}{d_2} \right) \right]^{-1}, \quad (19)$$

with $A = 0.0300$ MeV^{-1} fm, $B = 0.0061$ MeV^{-1} fm, $d_1 = 3.30$ fm, and $d_2 = 0.65$ fm. Note that where $b = 1$, ξ and s turn out to be the same quantities. This model was very successful in explaining the barrier heights, positions, and cross sections over a wide range of incident energies and masses of colliding nuclei. We labeled this potential Bass 77.

G. Bass 1980 (Bass 80)

The above potential form was further improved by Bass [14]. Here $\Phi(s = r - R_1 - R_2)$ is now given as:

$$\Phi(s) = \left[0.033 \exp\left(\frac{s}{3.5} \right) + 0.007 \exp\left(\frac{s}{0.65} \right) \right]^{-1}, \quad (20)$$

with central radius, R_i, as

$$R_i = R_s \left(1 - \frac{0.98}{R_s^2} \right) \quad (i = 1, 2), \quad (21)$$

where R_s is same as given by Eq. (4). We labeled this potential Bass 80.

H. Christensen and Winther 1976 (CW 76)

Christensen and Winther [18] derived the nucleus-nucleus interaction potential by analyzing the heavy-ion elastic-scattering data, based on the semiclassical arguments and the recognition that optical-model analysis of elastic scattering determines the real part of the interaction potential only in the vicinity of a characteristic distance. The nuclear part of the empirical potential due to Christensen and Winther is written as

$$V_N^{\text{CW76}}(r) = -50 \frac{R_1 R_2}{R_1 + R_2} \Phi(r - R_1 - R_2) \text{MeV}. \quad (22)$$

This form of the geometrical factor is similar to that of Bass77 with different radius parameters

$$R_i = 1.233 A_i^{1/3} - 0.978 A_i^{-1/3} \text{ fm} \quad (i = 1, 2). \quad (23)$$

The universal function $\Phi(s = r - R_1 - R_2)$ has the following form

$$\Phi(s) = \exp\left(-\frac{r - R_1 - R_2}{0.63} \right). \quad (24)$$

This model was tested for more than 60 reactions and we labeled it CW 76.

I. Broglia and Winther 1991 (BW 91)

A refined version of the above potential was derived by Broglia and Winther [14] by taking Woods-Saxon parametrization with subsidiary condition of being compatible with the value of the maximum nuclear force predicted by the proximity potential Prox 77. This refined potential resulted in

$$V_N^{\text{BW91}}(r) = -\frac{V_0}{1 + \exp\left(\frac{r - R_0}{0.63} \right)} \text{MeV}; \quad (25)$$

$$\text{with } V_0 = 16\pi \frac{R_1 R_2}{R_1 + R_2} \gamma a, \quad (26)$$

here $a = 0.63$ fm and

$$R_0 = R_1 + R_2 + 0.29. \quad (27)$$

Here radius R_i has the form

$$R_i = 1.233A_i^{1/3} - 0.98A_i^{-1/3} \text{ fm} \quad (i = 1, 2). \quad (28)$$

The form of the surface energy coefficient γ is quite similar to the one used in Prox 77 with slight difference

$$\gamma = \gamma_o \left[1 - k_s \left(\frac{N_p - Z_p}{A_p} \right) \left(\frac{N_t - Z_t}{A_t} \right) \right], \quad (29)$$

where $\gamma_0 = 0.95 \text{ MeV/fm}^2$ and $k_s = 1.8$. Note that the second term used in this potential gives different results when the projectile is symmetric ($N = Z$) and the target is asymmetric ($N > Z$). This form will also give different results for larger mass asymmetry η_A. Note that the radius used in this potential has same form like that of Bass with different constants. We labeled this potential BW 91.

J. Aage Winther (AW 95)

Winther adjusted the parameters of the above potential through an extensive comparison with experimental data for heavy-ion elastic scattering. This refined adjustment to slight different values of "a" and R_i as [19]

$$a = \left[\frac{1}{1.17\left(1 + 0.53\left(A_1^{-1/3} + A_2^{-1/3}\right)\right)} \right] \text{ fm} \quad (30)$$

and

$$R_i = 1.20A_i^{1/3} - 0.09 \text{ fm} \quad (i = 1, 2). \quad (31)$$

Here, $R_0 = R_1 + R_2$ only. We labeled this potential as AW 95.

K. Ngô 1980 (Ngô 80)

In earlier attempts, based on the microscopic picture of a nucleus and on the idea of energy-density formalism, the potential from Ngô and collaborators enjoys special status [25]. In this model, calculations of the ion-ion potential are performed within the framework of energy-density formalism due to Bruckener *et al.*, using a sudden approximation [32]. The need for Hartree-Fock densities as input in this model limited its scope. This not only made calculations tedious but also hindered its application to heavier nuclei. The above-stated parametrization was improved by H. Ngô and Ch. Ngô [21] by using a Fermi-density distribution for nuclear densities as

$$\rho_{n,p}(r) = \frac{\rho_{n,p}(0)}{1 + \exp[(r - C_{n,p})/0.55]}, \quad (32)$$

where C represents the central radius of the distribution and is defined in Prox 77 [see Eq. (3) with $b = 1$ fm]. Here $\rho_{n,p}(0)$ is given by

$$\rho_n(0) = \frac{3}{4\pi} \frac{N}{A} \frac{1}{r_{0_n}^3}; \quad \rho_p(0) = \frac{3}{4\pi} \frac{Z}{A} \frac{1}{r_{0_p}^3}. \quad (33)$$

Ngô parameterized the nucleus-nucleus interaction potential in the spirit of proximity concept. The interaction potential can be divided into the geometrical factor and a universal function. The nuclear part of the parameterized potential is

written as [21]

$$V_N^{\text{Ngo80}}(r) = \overline{R}\Phi(r - C_1 - C_2) \text{ MeV}, \quad (34)$$

where $\overline{R}$ is defined by Eq. (2). Now the nuclear radius R_i reads as

$$R_i = \frac{NR_{n_i} + ZR_{p_i}}{A_i} \quad (i = 1, 2). \quad (35)$$

The equivalent sharp radius for protons and neutrons are given as

$$R_{p_i} = r_{0_{p_i}} A_i^{1/3}; \quad R_{n_i} = r_{0_{n_i}} A_i^{1/3}, \quad (36)$$

with

$$r_{0_{p_i}} = 1.128 \text{ fm}; \quad r_{0_{n_i}} = 1.1375 + 1.875 \times 10^{-4} A_i \text{ fm}. \quad (37)$$

The above different radius formulas for the neutrons and protons take isotopic dependence into account. The universal function $\Phi(s = r - C_1 - C_2)$ (in MeV/fm) is noted by

$$\Phi(s) = \begin{cases} -33 + 5.4(s - s_0)^2, & \text{for } s < s_0, \\ -33 \exp\left[-\frac{1}{5}(s - s_0)^2\right], & \text{for } s \geqslant s_0, \end{cases} \quad (38)$$

and $s_0 = -1.6$ fm. We labeled this potential Ngô 80.

L. New Denisov Potential (Denisov DP)

Denisov [20] performed numerical calculations and parametrized the potential based on 7140 pair within semimicroscopic approximation. In total, 119 spherical or near spherical nuclei along the β-stability line from ^{16}O to ^{212}Po were taken. The potential is evaluated for any nucleus-nucleus combinations at 15 distances between ions around the touching point. By using this database, a simple analytical expression for the nuclear part of the interaction potential $V_N(r)$ between two spherical nuclei is presented as

$$V_N(r) = -1.989843 \frac{R_1 R_2}{R_1 + R_2} \Phi(r - R_1 - R_2 - 2.65)$$
$$\times \left[1 + 0.003525139 \left(\frac{A_1}{A_2} + \frac{A_2}{A_1} \right)^{3/2} \right.$$
$$\left. - 0.4113263(I_1 + I_2) \right], \quad (39)$$

with

$$I_i = \frac{N_i - Z_i}{A_i} \quad (i = 1, 2). \quad (40)$$

The effective nuclear radius R_i is given as

$$R_i = R_{ip} \left(1 - \frac{3.413817}{R_{ip}^2} \right)$$
$$+ 1.284589 \left(I_i - \frac{0.4A_i}{A_i + 200} \right) (i = 1, 2), \quad (41)$$

where, proton radius R_{ip} is given by Eq. (8) and $\Phi(s = r - R_1 - R_2 - 2.65)$ is given by the following

complex form:

$$
\Phi(s) = \begin{cases}
1 - s/0.7881663 + 1.229218s^2 \\
-0.2234277s^3 - 0.1038769s^4 \\
-\frac{R_1 R_2}{R_1+R_2}(0.1844935s^2 + 0.07570101s^3) \\
+(I_1 + I_2)(0.04470645s^2 + 0.03346870s^3), \\
\text{for} \quad -5.65 \leqslant s \leqslant 0, \\
\big[1 - s^2\big[0.05410106\frac{R_1 R_2}{R_1+R_2}\exp\big(-\frac{s}{1.760580}\big) \\
-0.5395420(I_1 + I_2)\exp\big(-\frac{s}{2.424408}\big)\big]\big] \\
\times \exp\big(-\frac{s}{0.7881663}\big), \\
\text{for} \quad s \geqslant 0.
\end{cases}
\tag{42}
$$

Here A_i, N_i, Z_i, R_i, and R_{ip} are, respectively, the mass number, the number of neutrons, the number of protons, the effective nuclear radius, and the proton radius of the target and projectile. The above form of the universal function not only depends on the separation distance s but also has complex dependence on the mass as well as on the relative neutron excess content. The above parametrization is derived for different combinations of nuclei between ^{16}O and ^{212}Po.

As stated in subsection II D, a new radius formula has become available recently [22]. We here extend the above potential due to Denisov to include this radius in its parametrization. This modified new version of the potential is labeled as Denisov DP [12]. Note that this new implementation was reported to yield very close agreement (within 1%) with experimental data for symmetric colliding pairs [12].

If one looks on the different versions of potentials (Bass 73, Bass 77, Bass 80, and CW 76), one notices that although the form of the radius is different, it is still isospin independent. Further, the corresponding universal functions are also isospin independent. The newer versions of Winther (BW 91 and AW 95) have incorporated a γ similar to the one used in the Prox 77 potential with a slightly different form. Here isospin content is calculated separately for the target/projectile. The latest version of Ngô (Ngô 80) has some isospin dependence in the radius parameter. In most of the above-mentioned potentials, modifications are made either through the surface energy coefficients or via nuclear radii. Both of these technical parameters can have sizable effects on the outcome of a reaction [33].

Using the above sets of models, the nuclear part of the interaction potential is calculated. By adding the Coulomb potential to a nuclear part, one can compute the total potential $V_T(r)$ for spherical colliding pairs as

$$V_T(r) = V_N(r) + V_C(r), \tag{43}$$

$$= V_N(r) + \frac{Z_1 Z_2 e^2}{r}. \tag{44}$$

Since the fusion happens at a distance larger than the touching configuration of colliding pair, the above form of the Coulomb potential is justified. One can extract the barrier height V_B^{theor} and barrier position R_B^{theor} using the following conditions

$$
\left.\frac{dV_T(r)}{dr}\right|_{r=R_B^{\text{theor}}} = 0; \quad \text{and} \quad \left.\frac{d^2V_T(r)}{dr^2}\right|_{r=R_B^{\text{theor}}} \leqslant 0.
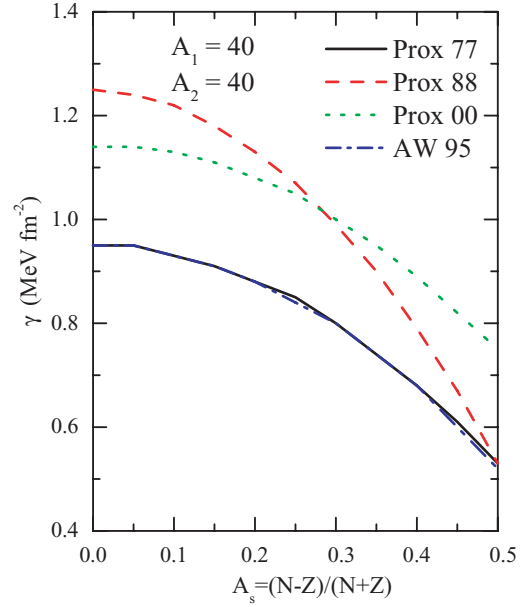\tag{45}
$$

FIG. 1. (Color online) The variation of the surface energy coefficient γ (MeV fm^{-2}) with asymmetry parameter A_s. We display the results using γ from Prox 77, Prox 88, Prox 00, and AW 95 for masses of reacting partner $A_1 = A_2 = 40$ units.

The knowledge of the shape of the potential as well as barrier position and height allows one to calculate the fusion cross section at a microscopic level. To study the fusion cross sections, we shall use the model given by Wong [34]. In this formalism, the cross section for complete fusion is given by

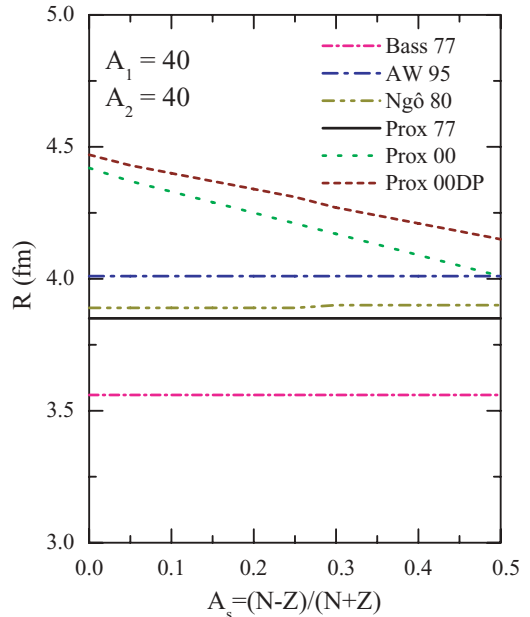$$\sigma_{\text{fus}} = \frac{\pi}{k^2} \sum_{l=0}^{l_{\max}} (2l + 1) \, T_l(E_{\text{c.m.}}), \tag{46}$$

FIG. 2. (Color online) Same as Fig. 1 but for various radii used in the literature.
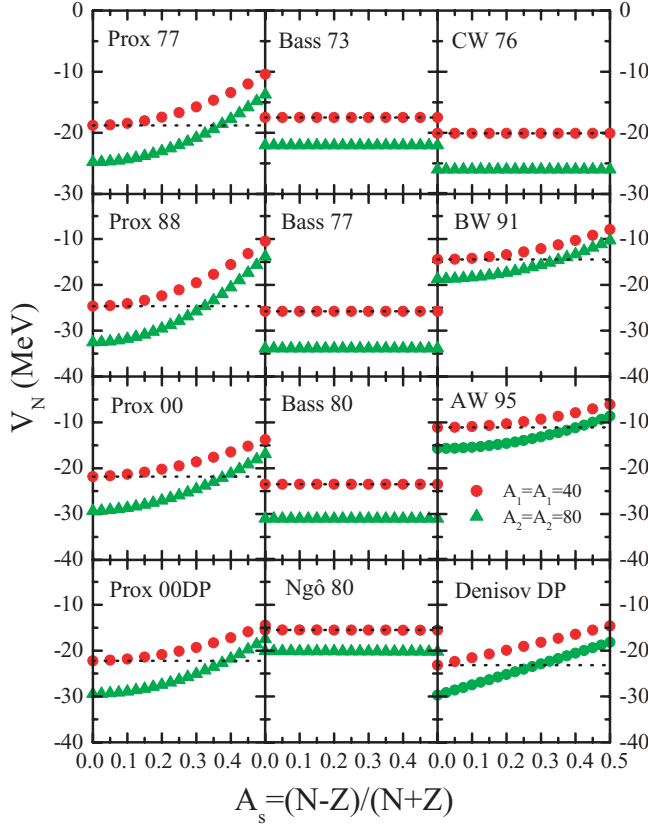
FIG. 3. (Color online) The strength of the nuclear potential V_N (MeV) calculated at a distance equal to $C_1 + C_2 + 1$ fm as a function of asymmetry parameter A_s for the reacting partners having masses $A_1 = A_2 = 40$ and $A_1 = A_2 = 80$ units. Here C_i denotes the central radius [12]. The dotted lines denote the value of the potential at $A_s = 0.0$ (for $A_1 = A_2 = 40$ only) using proximity potentials.

where $k = \sqrt{\frac{2\mu E}{\hbar^2}}$ and μ is the reduced mass. The center-of-mass energy is denoted by $E_{\text{c.m.}}$. In the above formula, $l_{\max}$ corresponds to the largest partial wave for which a pocket still exists in the interaction potential and $T_l(E_{\text{c.m.}})$ is the energy-dependent barrier penetration factor and is given by

$$T_l(E_{\text{c.m.}}) = \left\{ 1 + \exp\left[\frac{2\pi}{\hbar\omega_l} \left(V_{B_l}^{\text{theor}} - E_{\text{c.m.}} \right) \right] \right\}^{-1}, \quad (47)$$

where $\hbar\omega_l$ is the curvature of the inverted parabola. If we assume that the barrier position and width are independent of l, the fusion cross section reduces to

$$\sigma_{\text{fus}}(\text{mb}) = \frac{10 R_B^{\text{theor}2} \hbar\omega_0}{2 E_{\text{c.m.}}} \ln \left\{ 1 + \exp\left[\frac{2\pi}{\hbar\omega_0} \left(E_{\text{c.m.}} - V_B^{\text{theor}} \right) \right] \right\}. \quad (48)$$

For $E_{\text{c.m.}} \gg V_B^{\text{theor}}$, the above formula reduces to well-known sharp cut-off formula

$$\sigma_{\text{fus}}(\text{mb}) = 10\pi R_B^{\text{theor}2} \left(1 - \frac{V_B^{\text{theor}}}{E_{\text{c.m.}}} \right), \quad (49)$$
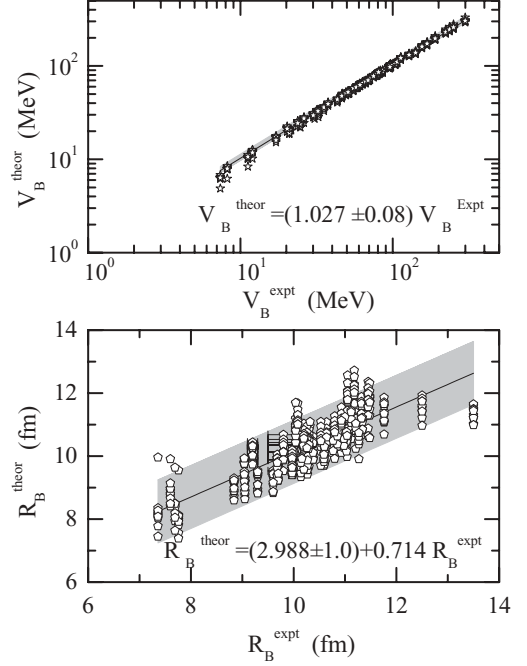

FIG. 4. The theoretical fusion barrier heights V_B (MeV) and positions R_B (fm) are displayed as a function of experimentally extracted values. The shaded area represents the region within which all 12 proximity potentials are able to reproduce experimental data.

whereas for $E_{\text{c.m.}} \ll V_B^{\text{theor}}$, the above formula reduces to

$$\sigma_{\text{fus}}(\text{mb}) = \frac{10 R_B^{\text{theor}2} \hbar\omega_0}{2 E_{\text{c.m.}}} \exp\left[\frac{2\pi}{\hbar\omega_0} \left(E_{\text{c.m.}} - V_B^{\text{theor}} \right) \right]. \quad (50)$$

We used Eq. (48) to calculate the fusion cross sections.

From the above brief discussion, it is clear that the main stress is made on the surface energy coefficients γ and nuclear radii to incorporate the isospin dependence in the nuclear potential. Definitely, the response of the isospin-dependent potentials will be different for asymmetric nuclei compared to symmetric nuclei. At intermediate energies, a strong effect was reported for the asymmetric reactions as well as for the mass dependence of the reaction [35].

III. RESULT AND DISCUSSION

The present study is conducted using a variety of the above-mentioned potentials. In total, 60 asymmetric reactions with compound mass between 29 and 294 (that have been experimentally explored) are taken for the present study. All nuclei considered here are assumed to be spherical in nature; however, deformation as well as orientation of the nuclei also affect the fusion barriers [26]. For uniform comparison of different models, we consider all colliding nuclei to be spherical. The lightest reaction taken is that of $^{12}\text{C} + ^{17}\text{O}$, whereas heaviest one is of $^{86}\text{Kr} + ^{208}\text{Pb}$. The asymmetry A_s of the colliding nuclei varies between 0.02 and 0.23. The other form of the asymmetry used in the literature is the mass asymmetry η_A [23,24]. In the present analysis, η_A varies between 0.0 and 0.97. Note that the nonzero value of A_s will involve complex interplay of the isospin degree of freedom
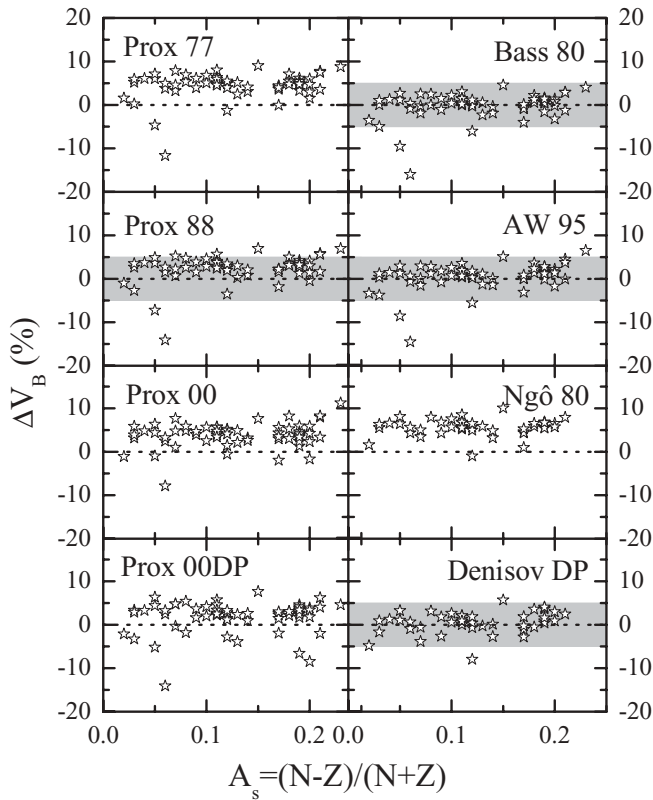
FIG. 5. The percentage difference $\Delta V_B(\%)$ of theoretical fusion barrier heights over experimental one as a function of asymmetry parameter A_s. Here only 60 reactions covering the whole mass and asymmetry range are taken. The shaded area is marked only for those potentials where the deviation is within $\pm 5\%$.

which has strong role at intermediate energies as well. The variation of η alters the physical outcome of a reaction with $\eta \approx 0.0$ leading to high dense matter and maximum collision volume, whereas a larger value of $\eta \approx 1.0$ will not be able to compress the matter to higher density [35].

As stated above, the isospin dependence of the different potentials enters via surface energy coefficient γ. In Fig. 1, we display the variation of γ (in MeV fm^{-2}) with asymmetry parameter A_s. Here we compare three versions of the surface energy coefficient γ used in Prox 77, Prox 88, and Prox 00 potentials along with the relation suggested in AW 95 potential. For the present analysis, the mass of the reacting partner is kept fixed equal to $A_1 = A_2 = 40$. The A_s was increased by increasing the neutrons and decreasing the protons. For example, $^{40}_{20}$Ca$_{20}$+$^{40}_{20}$Ca$_{20}$ has $A_s = 0.0$. For $A_s = 0.2$, we chose the reaction of $^{40}_{16}$S$_{24}$+$^{40}_{16}$S$_{24}$, whereas for $A_s = 0.4$, the reaction was $^{40}_{12}$Mg$_{28}$+$^{40}_{12}$Mg$_{28}$. In all cases, the mass of the reacting partner is kept fixed, whereas the ratio A_s is varied by converting the proton into neutrons. At the end of this series, we have the reaction of $^{40}_{10}$Ne$_{30}$+$^{40}_{10}$Ne$_{30}$ having $A_s = 0.5$. From the figure, we see that the surface energy coefficient γ used in the latest proximity potentials Prox 00/ Prox 00DP as well as in original version Prox 77 is less sensitive toward the asymmetry and isospin dependence, whereas the one used in the Prox 88 potential has a stronger dependence on the asymmetry of the reacting nuclei. The coefficient γ of AW 95 yields same results
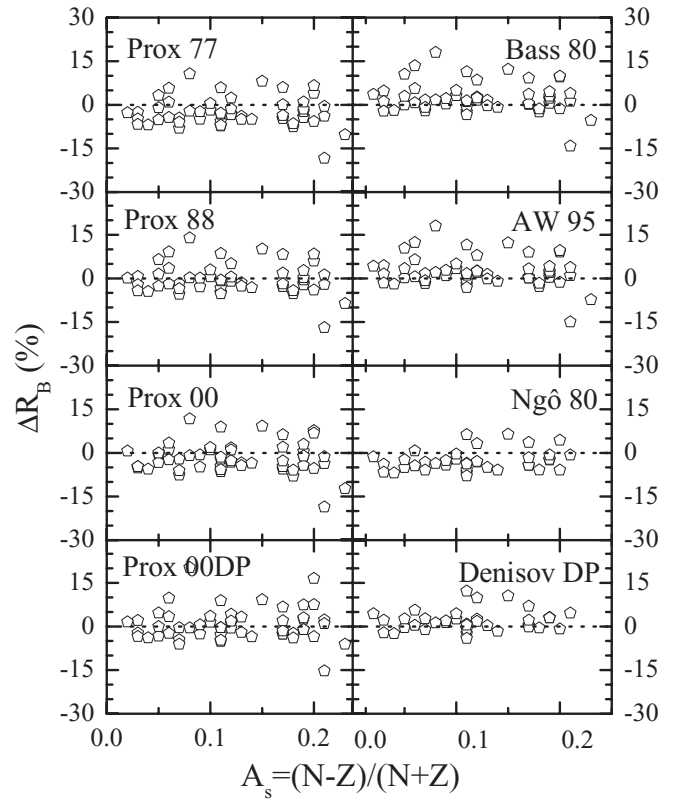
FIG. 6. Same as Fig. 5 but for percentage difference $\Delta R_B(\%)$.

like Prox 77. Since nuclear potential $V_N(r)$ depends directly on γ, one can conclude that the potentials calculated within Prox 88 and Prox 77 will be far less attractive for larger asymmetries compared to the one generated using Prox 00. When colliding nuclei are symmetric ($N = Z$; $A_s = 0.0$), such dependence does not play a role. In many studies [23], one finds that neutron excess leads to more attraction. In these studies, the total mass of the colliding pair is not fixed and, as a result, this dependence is more of mass dependence than of isospin dependence.

In Fig. 2, we display the dependence of different nuclear radii on the asymmetry parameter A_s. As noted above, this parameter also plays significant role in nuclear potential and finally in the barrier calculations. We show the dependence of different forms of nuclear radii used in various potentials on the asymmetry parameter. We see that the radius used in the Prox 77 (also in Prox 88) as well as in Bass versions (i.e., Bass 73, Bass 77, and Bass 80) and all versions from Winther (CW 76, BW 91, and AW 95) are independent of the asymmetry content, whereas the one used in the Prox 00, Prox 00DP (and Denisov DP), and Ngô 80 versions depends on the asymmetry content of the colliding pairs.

From Figs. 1 and 2, we see that both these parameters can lead to significant change in the nuclear potential and ultimately in the fusion barriers even if the universal function $\Phi(s)$ is kept the same. In Fig. 3, we display the nuclear part of the interaction potential $V_N(r)$ at a distance of $C_1 + C_2 + 1$ fm for the same sets of the reactions as depicted in Figs. 1 and 2. In addition, a series of heavier reacting partners with mass

$A_1 = A_2 = 80$ is also taken. We display four versions of proximity potential, three versions from Bass and Winther and one each of the latest versions of Ngô and Denisov. We see a systematic decrease in the attractive strength of the potentials with asymmetry content A_s. The decrease is stronger for the Prox 88 version compared to Prox 77, Prox 00, and Prox 00DP. The Bass 73, Bass 77, and Bass 80 versions of the potential are independent of the asymmetry content. One also notices a very weak dependence in the Ngô 80 potential. Two of the three versions of the Winther potential have significant dependence on the asymmetry of the reaction. The Winther 1976 potential, however, does not show such dependence due to the absence

of γ term in the potential. The Denisov DP potential also shows a linear decrease in the strength of the potential with asymmetry content. These variations are stronger for heavier colliding nuclei. This figure shows true isospin dependence of the nuclear potential as the mass of the colliding nuclei is kept fixed. All those potentials that do not depend on the asymmetry parameter A_s will not show any change in the structure.

We now shift from the systematic study to the study involving real nuclei. As stated above, here 60 reactions with A_s between 0.02 and 0.23 and η_A between 0.0 and 0.97 are taken. For all these reactions, experimental fusion barriers are known [2–11,36–58]. In Fig. 4, we display the fusion barrier

TABLE I. The fusion barrier heights V_B (in MeV) and positions R_B (in fm) using different proximity potentials for 60 asymmetric systems. The corresponding experimental values are also listed.

Reaction	Prox 77		Prox 88		Prox 00		Prox 00DP		Empirical		Ref.
	V_B	R_B	V_B	R_B	V_B	R_B	V_B	R_B	V_B	R_B	
^{7}Li+^{27}Al	6.52	7.78	6.34	8.03	6.80	7.45	6.34	8.08	7.38	7.36	[36]
^{12}C+^{17}O	8.22	7.56	7.98	7.81	8.46	7.39	7.93	7.92	8.20	7.76	[37]
^{11}B+^{27}Al	10.68	7.94	10.39	8.19	11.09	7.64	10.62	8.05	11.20	7.69	[36]
^{6}Li+^{59}Co	12.64	8.41	12.31	8.66	12.58	8.49	11.78	9.14	12.00	7.60	[38]
^{4}He+^{164}Dy	17.71	9.90	17.36	10.15	17.36	10.20	16.01	11.09	17.14	10.32	[39]
^{4}He+^{209}Bi	21.30	10.44	20.89	10.64	20.63	10.81	19.20	11.70	20.98	10.04	
									±0.05	±0.01	[40]
^{26}Mg+^{30}Si	25.61	8.64	24.97	8.89	25.05	8.86	24.71	9.01	24.80	9.05	[41]
^{6}He+^{238}U	22.06	11.22	21.69	11.42	22.56	10.97	21.21	11.74	20.28	12.50	[42]
^{6}Li+^{144}Sm	25.26	9.80	24.72	10.05	25.18	9.85	23.69	10.53	24.65	10.20	[43]
^{14}N+^{59}Co	28.19	8.83	27.50	9.08	28.13	8.87	27.37	9.16	26.13	9.60	[44]
^{7}Li+^{159}Tb	25.50	10.20	25.00	10.45	26.76	10.15	24.32	10.77	23.81	11.03	[39]
^{24}Mg+^{35}Cl	31.18	8.60	30.39	8.85	30.36	8.90	30.04	8.98	30.70	8.84	[5]
^{16}O+^{58}Ni	33.32	8.85	32.51	9.10	33.52	8.82	32.72	9.09	31.67	9.30	[45]
^{18}O+^{64}Ni	32.08	9.25	31.35	9.50	32.32	9.20	31.58	9.42	32.50	9.04	[3]
^{12}C+^{92}Zr	33.88	9.38	33.12	9.63	33.98	9.37	32.78	9.79	32.31	9.68	[45]
^{6}Li+^{208}Pb	31.17	10.57	30.59	10.77	31.11	10.60	29.49	11.25	30.10	11.00	[46]
^{16}O+^{72}Ge	36.79	9.22	35.94	9.42	36.80	9.23	35.96	9.45	35.40	9.70	[2]
^{36}S+^{48}Ca	44.63	9.51	43.65	9.76	44.67	9.55	43.70	9.78	43.30		[11]
^{10}Be+^{209}Bi	40.50	11.02	39.78	11.22	40.59	10.99	39.11	11.44	37.60	13.50	[47]
^{19}F+^{93}Nb	50.34	9.74	49.24	9.99	49.27	10.02	49.27	10.02	46.60	9.20	
									±0.10	±0.10	[48]
^{12}C+^{152}Sm	48.37	10.28	47.41	10.48	48.98	10.17	47.60	10.49	46.39	10.77	[39]
^{16}O+^{116}Sn	53.56	9.94	52.43	10.19	53.48	10.01	52.35	10.23	50.94	10.36	[49]
^{18}O+^{124}Sn	51.99	10.27	50.97	10.52	51.89	10.33	50.81	10.55	49.30	10.98	[50]
^{48}Ca+^{48}Ca	53.96	9.89	52.84	10.09	53.93	9.89	52.86	10.11	51.70	10.38	[9]
^{27}Al+^{70}Ge	57.62	9.59	56.34	9.84	57.74	9.58	57.74	9.58	55.10	10.20	[4]
^{40}Ca+^{48}Ti	61.67	9.46	60.27	9.71	60.71	9.64	60.71	9.64	58.17	9.97	
									±0.62	±0.07	[7]
^{35}Cl+^{54}Fe	62.04	9.46	60.62	9.71	60.85	9.66	60.27	9.79	58.59	10.14	[51]
^{37}Cl+^{64}Ni	64.41	9.82	63.03	10.07	64.02	9.91	63.37	10.05	60.60	10.59	[6]
^{46}Ti+^{46}Ti	67.15	9.56	65.64	9.81	66.34	9.70	65.38	9.87	63.30	10.27	[52]
^{12}C+^{204}Pb	60.73	10.84	59.61	11.09	60.96	10.85	59.08	11.22	57.55	11.34	[45]
^{16}O+^{144}Sm	64.16	10.31	62.86	10.56	64.01	10.38	62.47	10.63	61.03	10.85	[45]
^{40}Ar+^{58}Ni	68.84	9.72	67.33	9.97	67.93	9.92	67.93	9.92	66.32	10.16	[39]
^{37}Cl+^{73}Ge	72.43	10.00	70.91	10.25	71.88	10.11	70.74	10.30	69.20	10.60	[53]
^{28}Si+^{92}Zr	74.52	10.00	72.95	10.25	72.72	10.30	72.35	10.34	70.93	10.19	[45]
^{16}O+^{186}W	73.09	10.86	71.74	11.06	71.39	11.18	70.03	11.40	68.87	11.12	[45]
^{48}Ti+^{58}Ni	82.70	9.89	80.91	10.14	81.34	10.13	81.34	10.13	78.80	9.80	
									±0.30	±0.30	[8]

TABLE I. (*Continued.*)

Reaction	Prox 77		Prox 88		Prox 00		Prox 00DP		Empirical		Ref.
	V_B	R_B	V_B	R_B	V_B	R_B	V_B	R_B	V_B	R_B	
^{32}S+^{89}Y	82.52	10.06	80.78	10.31	81.38	10.23	80.62	10.36	77.77	10.30	[45]
^{36}S+^{90}Zr	82.99	10.30	81.30	10.55	82.35	10.41	81.10	10.60	79.00	10.64	[54]
^{16}O+^{208}Pb	79.38	11.09	77.96	11.29	79.30	11.13	77.78	11.35	74.90	11.76	[46]
^{35}Cl+^{92}Zr	88.58	10.25	86.75	10.50	87.64	10.39	86.41	10.56	82.94	10.20	[45]
^{28}Si+^{120}Sn	89.43	10.49	87.65	10.69	88.12	10.65	88.12	10.65	85.89	11.04	[55]
^{19}F+^{197}Au	85.70	11.15	84.16	11.35	85.33	11.20	85.33	11.20	81.61	11.32	[45]
^{16}O+^{238}U	86.86	11.39	85.37	11.59	87.46	11.30	85.81	11.56	80.81	11.45	[45]
^{35}Cl+^{106}Pd	99.86	10.48	97.85	10.68	98.75	10.62	97.45	10.74	94.30	11.27	[56]
^{58}Ni+^{60}Ni	102.83	10.16	100.67	10.41	102.07	10.26	102.07	10.26	96.00	10.26	[45]
^{32}S+^{116}Sn	101.78	10.49	99.75	10.74	100.65	10.64	99.73	10.76	97.36	10.80	[49]
^{40}Ca+^{90}Zr	103.60	10.30	101.46	10.55	102.57	10.43	102.10	10.48	96.88	10.53	[45]
^{48}Ca+^{96}Zr	99.33	10.80	97.46	11.00	98.73	10.90	97.28	11.04	95.90	11.21	[10]
^{28}Si+^{144}Sm	108.00	10.78	105.90	10.98	105.40	11.04	105.03	11.13	103.89	10.93	[45]
^{50}Ti+^{93}Nb	112.74	10.71	110.54	10.96	111.25	10.87	110.38	10.99	106.90		[57]
^{40}Ca+^{124}Sn	123.11	10.90	120.78	11.10	121.55	11.01	121.55	11.01	112.93	10.08	[45]
^{28}Si+^{208}Pb	133.90	11.56	131.59	11.76	131.10	11.79	131.10	11.79	128.07	11.45	[45]
^{40}Ar+^{165}Ho	141.27	11.49	138.78	11.69	138.61	11.71	138.61	11.71	141.38	11.48	[39]
^{32}S+^{232}Th	163.08	11.92	160.39	12.12	162.32	11.94	160.97	12.02	155.73	11.18	[45]
^{40}Ca+^{192}Os	174.70	11.71	171.71	11.96	173.90	11.74	173.07	11.79	168.07	11.05	[45]
^{48}Ti+^{208}Pb	200.34	12.18	197.08	12.38	197.08	12.34	197.08	12.34	190.10		[58]
^{56}Fe+^{208}Pb	233.61	12.33	229.84	12.58	229.74	12.45	229.74	12.45	223.00		[58]
^{64}Ni+^{208}Pb	247.56	12.56	243.66	12.76	245.68	12.53	245.68	12.53	236.00		[58]
^{70}Zn+^{208}Pb	262.60	12.71	258.53	12.91	259.01	12.76	259.01	12.76	250.60		[58]
^{86}Kr+^{208}Pb	308.05	12.99	303.40	13.24	306.16	12.92	304.56	12.98	299.20		[58]

TABLE II. Fusion barrier heights V_B (in MeV) and positions R_B (in fm) are displayed using other different proximity potentials for 60 asymmetric systems. The limited numbers of reactions in certain cases are due to the restriction posed in different potentials.

Reaction	Bass 80		Ngo 80̊		AW 95		Denisov DP	
	V_B	R_B	V_B	R_B	V_B	R_B	V_B	R_B
^{7}Li+^{27}Al	6.20	8.35	–	–	6.31	8.27	–	–
^{12}C+^{17}O	7.79	8.13	–	–	7.89	8.10	–	–
^{11}B+^{27}Al	10.13	8.50	–	–	10.24	8.49	–	–
^{6}Li+^{59}Co	12.00	8.97	–	–	12.14	8.97	–	–
^{4}He+^{164}Dy	16.87	10.51	–	–	17.12	10.44	–	–
^{4}He+^{209}Bi	20.30	11.00	–	–	20.62	10.95	–	–
^{26}Mg+^{30}Si	24.33	9.20	25.65	8.76	24.42	9.20	23.84	9.29
^{6}He+^{238}U	21.10	11.83	–	–	21.60	11.59	–	–
^{6}Li+^{144}Sm	24.08	10.36	–	–	24.34	10.34	–	–
^{14}N+^{59}Co	26.79	9.40	–	–	26.90	9.43	–	–
^{7}Li+^{159}Tb	24.33	10.76	–	–	24.67	10.72	–	–
^{24}Mg+^{35}Cl	29.61	9.16	31.19	8.72	29.67	9.21	29.21	9.23
^{16}O+^{58}Ni	31.69	9.41	33.42	8.94	31.78	9.44	31.14	9.50
^{18}O+^{64}Ni	30.53	9.81	32.18	9.33	30.70	9.76	29.91	9.93
^{12}C+^{92}Zr	32.26	9.94	–	–	32.43	9.93	–	–
^{6}Li+^{208}Pb	29.72	11.14	–	–	30.08	11.11	–	–
^{16}O+^{72}Ge	35.02	9.73	36.92	9.29	35.14	9.79	34.46	9.83
^{36}S+^{48}Ca	42.48	10.07	44.69	9.59	42.69	10.04	42.11	10.09
^{10}Be+^{209}Bi	38.70	11.59	–	–	39.29	11.48	–	–
^{19}F+^{93}Nb	48.01	10.25	50.57	9.78	48.24	10.26	47.56	10.32
^{12}C+^{152}Sm	46.13	10.79	–	–	46.45	10.82	–	–
^{16}O+^{116}Sn	51.11	10.45	53.85	9.97	51.36	10.50	50.61	10.55
^{18}O+^{124}Sn	49.57	10.83	52.18	10.34	49.98	10.80	49.04	10.93

TABLE II. (*Continued.*)

Reaction	Bass 80		Ngo $\hat{8}0$		AW 95		Denisov DP	
	V_B	R_B	V_B	R_B	V_B	R_B	V_B	R_B
^{48}Ca+^{48}Ca	51.39	10.40	54.06	9.94	51.74	10.39	51.13	10.42
^{27}Al+^{70}Ge	54.97	10.11	57.86	9.60	55.13	10.12	54.77	10.09
^{40}Ca+^{48}Ti	58.83	9.97	61.90	9.47	58.91	9.99	58.76	9.93
^{35}Cl+^{54}Fe	59.18	9.92	62.28	9.47	59.28	9.98	59.11	9.92
^{37}Cl+^{64}Ni	61.47	10.33	64.67	9.87	61.71	10.37	61.37	10.33
^{46}Ti+^{46}Ti	64.10	10.07	67.45	9.56	64.21	10.07	64.09	10.02
^{12}C+^{204}Pb	58.04	11.40	57.86	9.60	58.53	11.38	55.13	10.12
^{16}O+^{144}Sm	61.34	10.82	64.59	10.31	61.68	10.83	60.85	10.88
^{40}Ar+^{58}Ni	65.75	10.23	69.19	9.71	65.91	10.22	65.71	10.20
^{37}Cl+^{73}Ge	69.19	10.51	72.81	9.98	69.48	10.48	69.21	10.49
^{28}Si+^{92}Zr	71.21	10.51	74.96	9.97	71.44	10.53	71.32	10.45
^{16}O+^{186}W	69.86	11.37	73.44	10.85	70.36	11.34	69.47	11.45
^{48}Ti+^{58}Ni	79.08	10.35	83.24	9.87	79.28	10.43	79.28	10.35
^{32}S+^{89}Y	78.91	10.52	83.07	10.03	79.15	10.59	79.18	10.50
^{36}S+^{90}Zr	79.40	10.76	83.56	10.26	79.82	10.76	79.54	10.73
^{16}O+^{208}Pb	75.92	11.60	79.76	11.07	76.52	11.60	75.55	11.66
^{35}Cl+^{92}Zr	84.76	10.71	89.22	10.16	85.09	10.71	85.11	10.65
^{28}Si+^{120}Sn	85.56	10.95	90.04	10.39	85.94	10.93	85.98	10.86
^{19}F+^{197}Au	82.04	11.66	86.19	11.07	82.76	11.60	81.92	11.67
^{16}O+^{238}U	83.12	11.90	87.20	11.37	83.85	11.88	82.77	11.98
^{35}Cl+^{106}Pd	95.67	10.89	100.71	10.38	96.09	10.92	96.24	10.81
^{58}Ni+^{60}Ni	98.53	10.56	103.77	10.02	98.80	10.61	99.09	10.53
^{32}S+^{116}Sn	97.53	10.95	102.68	10.39	97.93	10.98	98.18	10.85
^{40}Ca+^{90}Zr	99.28	10.71	104.55	10.15	99.58	10.75	99.93	10.66
^{48}Ca+^{96}Zr	95.05	11.26	100.03	10.74	95.87	11.23	95.61	11.19
^{28}Si+^{144}Sm	103.60	11.19	109.04	10.61	104.12	11.20	104.31	11.12
^{50}Ti+^{93}Nb	108.10	11.17	113.83	10.59	108.77	11.13	108.87	11.06
^{40}Ca+^{124}Sn	118.07	11.31	124.29	10.73	118.66	11.31	119.36	11.14
^{28}Si+^{208}Pb	128.56	11.97	135.03	11.37	129.53	11.92	130.06	11.79
^{40}Ar+^{165}Ho	135.70	11.90	142.75	11.29	136.97	11.86	137.38	11.73
^{32}S+^{232}Th	156.86	12.28	164.65	11.67	158.17	12.25	–	–
^{40}Ca+^{192}Os	168.22	12.07	176.93	11.45	169.44	12.05	171.15	11.82
^{48}Ti+^{208}Pb	193.15	12.49	203.09	11.86	195.26	12.44	196.99	12.15
^{56}Fe+^{208}Pb	225.72	12.59	237.53	11.89	228.16	12.52	230.95	12.18
^{64}Ni+^{208}Pb	239.28	12.81	251.83	12.10	242.40	12.68	245.24	12.31
^{70}Zn+^{208}Pb	253.99	12.92	267.37	12.20	257.54	12.78	260.75	12.37
^{86}Kr+^{208}Pb	298.65	13.15	–	–	303.25	12.98	308.13	12.32

heights V_B and barrier positions R_B versus experimental values for the above-mentioned reactions involving 12 different potentials. For the clarity of the figure, only 60 asymmetric reactions studied experimentally and covering the whole range of the mass and asymmetry are displayed. We see no clear difference with fusion barrier heights and positions. The fusion barrier heights can be reproduced within ±10% in all cases on the average. Due to the large uncertainty in the fusion barrier positions, no definite trend and conclusion can be drawn as is observed for the symmetric colliding nuclei [12]. To further understand the role of isospin content, we display, in Fig. 5, the percentage difference of the fusion barrier heights $\Delta V_B(\%)$ defined as

$$\Delta V_B(\%) = \frac{V_B^{\text{theor}} - V_B^{\text{expt}}}{V_B^{\text{expt}}} \times 100, \qquad (51)$$

verses asymmetry parameter A_s. In some cases, only the latest versions of the potential are shown. Interestingly, we see that Prox 77 and Ngô 80 fail to reproduce the barrier heights satisfactorily, whereas Prox 88, Bass 80, AW 95, Prox 00DP, and Denisov DP do a far better job compared to other potentials. We do not see any systematic deviation/improvement in the fusion barrier heights with the asymmetry of the colliding nuclei. We see that the potentials Prox 88, Bass 80, AW 95, and Denisov DP can reproduce the empirical barrier heights within ±5% (see the shaded regions in Fig. 5), whereas others need ±10% to produce the same result.

The comparison of the fusion barrier positions outcome is shown in Fig. 6. We see that due to large uncertainty in the measurements of fusion barrier positions, a large deviation is seen and all the models are able to reproduce the results within ±10%. The precise values of the fusion barrier heights
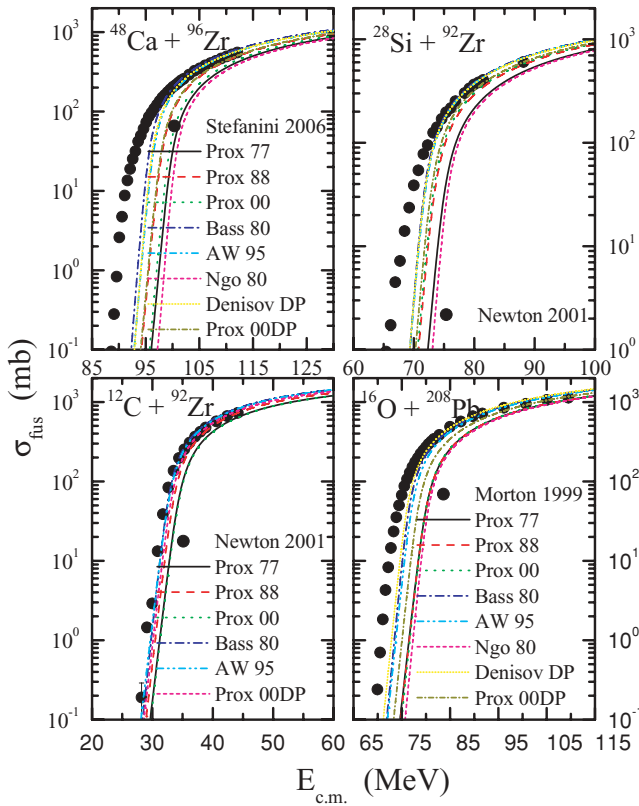
FIG. 7. (Color online) The fusion cross sections $\sigma_{\rm fus}$ (mb) as a function of center-of-mass energy $E_{\rm c.m.}$ (MeV). For clarity, only latest versions of different proximity potentials are shown. The experimental data are taken from Stefanini 2006 [10], Newton 2001 [59], and Morton 1999 [60].

V_B (in MeV) and positions R_B (in fm) are shown in Tables I and II for 60 asymmetric colliding nuclei involving significant variations of asymmetry A_s as well as mass asymmetry η_A. The experimental (or empirical) barriers displayed in Tables I and II and in Figs. 4–6 are obtained by fitting the cross sections in the approach, when shapes of both colliding nuclei are spherical. A large number of experimental data are available for different reactions; however, we restrict ourselves to the latest one only.

In Figs. 7 and 8, we display the fusion cross sections $\sigma_{\rm fus}$ (in mb) as a function of center-of-mass energy $E_{\rm c.m.}$ for the reactions of ^{48}Ca+^{96}Zr [10], ^{28}Si+^{92}Zr [59], ^{12}C+^{92}Zr [59], ^{16}O+^{208}Pb [60] (in Fig. 7) and ^{16}O+^{50}Ti [61], ^{16}O+^{112}Sn [49], ^{16}O+^{116}Sn [49], and ^{16}O+^{120}Sn [55] (in Fig. 8). Here the latest versions of proximity parametrizations along with original proximity potential and its modifications are shown for clarity. As we see, Bass 80, Denisov DP, and AW 95 do a better job for all the systems, whereas Prox 77 and Ngô 80 fail to come closer to the experimental data. The above results are in agreement with the one obtained for symmetric colliding nuclei [12].
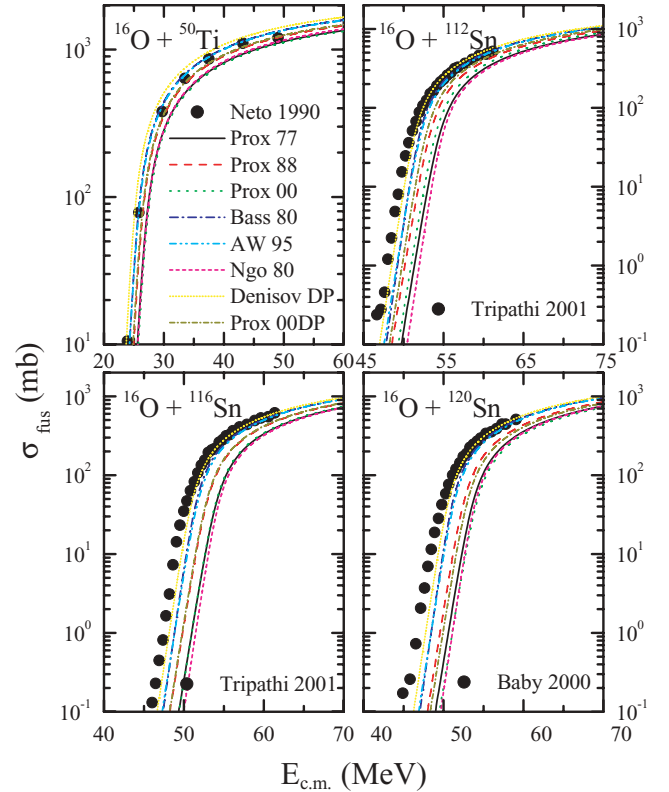
FIG. 8. (Color online) Same as Fig. 7 but for different systems explained in the text. The experimental data are taken from Neto 1990 [61], Tripathi 2001 [49], and Baby 2000 [55].

IV. SUMMARY

We performed a systematic study of the role of isospin dependence on fusion barriers by employing as many as 12 different proximity-based potentials. Some of the potentials have isospin dependence via the surface energy coefficient as well as via nuclear radius. We noted that the nuclear part of the potential becomes more shallow with asymmetry of the reaction. On the other hand, a detailed comparison of different potentials does not show any preference for the isospin-dependent potential. Our comparison for 60 reactions reveals that all models can explain the fusion barrier heights within ±10%. The potentials from Prox 88, Bass 80, AW 95, and Denisov DP perform better than others. The fusion cross sections are nicely explained by Bass 80, AW 95, and Denisov DP potentials at below as well as above barrier energies.

ACKNOWLEDGMENTS

[1] L. F. Canto, P. R. S. Gomes, R. Donangelo, and M. S. Hussein, Phys. Rep. **424**, 1 (2006).

[2] E. F. Aguilera, J. J. Kolata, and R. J. Tighe, Phys. Rev. C **52**, 3103 (1995).

[3] C. P. Silva, D. Pereira, L. C. Chamon, E. S. Rossi, G. Ramirez, A. M. Borges, and C. E. Aguiar, Phys. Rev. C **55**, 3155 (1997).

[4] E. F. Aguilera, J. J. Vega, J. J. Kolata, A. Morsad, R. G. Tighe, and X. J. Kong, Phys. Rev. C **41**, 910 (1990).

[5] S. Cavallaro *et al.*, Nucl. Phys. A **513**, 174 (1990).

[6] J. J. Vega, E. F. Aguilera, G. Murillo, J. J. Kolata, A. Morsad, and X. J. Kong, Phys. Rev. C **42**, 947 (1990).

[7] A. A. Sonzogni, J. D. Bierman, M. P. Kelly, J. P. Lestone, J. F. Liang, and R. Vandenbosch, Phys. Rev. C **57**, 722 (1998).

[8] A. M. Vinodkumar *et al.*, Phys. Rev. C **53**, 803 (1996).

[9] M. Trotta, A. M. Stefanini, L. Corradi, A. Gadea, F. Scarlassara, S. Beghini, and G. Montagnoli, Phys. Rev. C **65**, 011601(R) (2001).

[10] A. M. Stefanini *et al.*, Phys. Rev. C **73**, 034606 (2006).

[11] A. M. Stefanini *et al.*, Phys. Rev. C **78**, 044607 (2008).

[12] I. Dutt and R. K. Puri, Phys. Rev. C **81**, 044615 (2010).

[13] J. Blocki, J. Randrup, W. J. Świątecki, and C. F. Tsang, Ann. Phys. (NY) **105**, 427 (1977).

[14] W. Reisdorf, J. Phys. G: Nucl. Part. Phys. **20**, 1297 (1994).

[15] W. D. Myers and W. J. Świątecki, Phys. Rev. C **62**, 044610 (2000).

[16] R. Bass, Phys. Lett. B **47**, 139 (1973); Nucl. Phys. A **231**, 45 (1974).

[17] R. Bass, Phys. Rev. Lett. **39**, 265 (1977).

[18] P. R. Christensen and A. Winther, Phys. Lett. B **65**, 19 (1976).

[19] A. Winther, Nucl. Phys. A **594**, 203 (1995).

[20] V. Y. Denisov, Phys. Lett. B **526**, 315 (2002).

[21] H. Ngô and C. Ngô, Nucl. Phys. A **348**, 140 (1980).

[22] G. Royer and R. Rousseau, Eur. Phys. J. A **42**, 541 (2009).

[23] R. K. Puri *et al.*, Eur. Phys. J. A **23**, 429 (2005); R. Arora *et al.*, *ibid.* **8**, 103 (2000); R. K. Puri *et al.*, *ibid.* **3**, 277 (1998); R. K. Puri, P. Chattopadhyay, and R. K. Gupta, Phys. Rev. C **43**, 315 (1991); R. K. Puri and R. K. Gupta, *ibid.* **45**, 1837 (1992); N. K. Dhiman *et al.*, Acta Phys. Pol. B **38**, 2133 (2007); **37**, 1855 (2006).

[24] R. K. Gupta, S. Singh, R. K. Puri, and W. Scheid, Phys. Rev. C **47**, 561 (1993); R. K. Gupta *et al.*, J. Phys. G: Nucl. Part. Phys. **18**, 1533 (1992); S. S. Malik *et al.*, Pramana: J. Phys. **32**, 419 (1989); R. K. Puri *et al.*, Europhys. Lett. **9**, 767 (1989); J. Phys. G: Nucl. Part. Phys. **18**, 903 (1992).

[25] C. Ngô, B. Tamain, M. Beiner, R. J. Lombard, D. Mas, and H. H. Deubler, Nucl. Phys. A **252**, 237 (1975).

[26] V. Y. Denisov and N. A. Pilipenko, Phys. Rev. C **76**, 014602 (2007); A. S. Umar and V. E. Oberacker, *ibid.* **77**, 064605 (2008); M. Ismail, W. M. Seif, and M. M. Botros, Nucl. Phys. A **828**, 333 (2009).

[27] P. Möller and J. R. Nix, Nucl. Phys. A **361**, 117 (1981).

[28] P. Möller, J. R. Nix, W. D. Myers, and W. J. Świątecki, At. Data Nucl. Data Tables **59**, 185 (1995).

[29] W. D. Myers and W. J. Światecki, Ann. Phys. **55**, 395 (1969); Nucl. Phys. A **336**, 267 (1980).

[30] C. W. de Jager, H. de Vries, and C. de Vries, At. Data Nucl. Data Tables **14**, 479 (1974); H. de Vries, C. W. de Jager, and C. de Vries, *ibid.* **36**, 495 (1987).

[31] B. Nerlo-Pomorska and K. Pomorski, Z. Phys. A **348**, 169 (1994).

[32] K. A. Brueckner, J. R. Buchler, and M. Kelly, Phys. Rev. **173**, 944 (1968).

[33] I. Dutt and R. K. Puri, Phys. Rev. C **81**, 047601 (2010).

[34] C. Y. Wong, Phys. Lett. B **42**, 186 (1972); Phys. Rev. Lett. **31**, 766 (1973).

[35] R. K. Puri *et al.*, Nucl. Phys. A **575**, 733 (1994); R. K. Puri and C. Hartnack, and J. Aichelin, Phys. Rev. C **54**, R28 (1996); S. Kumar, M. K. Sharma, R. K. Puri, K. P. Singh, and I. M. Govil, *ibid.* **58**, 3494 (1998); J. Singh, S. Kumar, and R. K. Puri *et al.*, *ibid.* **62**, 044617 (2000); R. K. Puri *et al.*, J. Comput. Phys. **162**, 245 (2000); S. Kumar, S. Kumar, and R. K. Puri, Phys. Rev. C **78**, 064602 (2008); Y. K. Vermani, S. Goyal, and R. K. Puri, J. Phys. G: Nucl. Part. Phys. **37**, 015105 (2010); Y. K. Vermani *et al.*, Phys. Rev. C **79**, 064613 (2009); J. Phys. G: Nucl. Part. Phys. **36**, 105103 (2009); Europhys. Lett. **85**, 62001 (2009); A. Sood and R. K. Puri, Phys. Rev. C **79**, 064618 (2009).

[36] I. Padron *et al.*, Phys. Rev. C **66**, 044608 (2002).

[37] R. J. Tighe, J. J. Kolata, M. Belbot, and E. F. Aguilera, Phys. Rev. C **47**, 2699 (1993).

[38] C. Beck *et al.*, Phys. Rev. C **67**, 054602 (2003).

[39] L. C. Vaz, J. M. Alexander, and G. R. Satchler, Phys. Rep. **69**, 373 (1981).

[40] J. J. Kolata *et al.*, Phys. Rev. Lett. **81**, 4580 (1998).

[41] A. Morsad, J. J. Kolata, R. J. Tighe, X. J. Kong, E. F. Aguilera, and J. J. Vega, Phys. Rev. C **41**, 988 (1990).

[42] M. Trotta *et al.*, Phys. Rev. Lett. **84**, 2342 (2000).

[43] P. K. Rath *et al.*, Phys. Rev. C **79**, 051601(R) (2009).

[44] P. R. S. Gomes *et al.*, Nucl. Phys. A **534**, 429 (1991).

[45] J. O. Newton, R. D. Butt, M. Dasgupta, D. J. Hinde, I. I. Gontchar, C. R. Morton, and K. Hagino, Phys. Rev. C **70**, 024605 (2004).

[46] Z. H. Liu *et al.*, Eur. Phys. J. A **26**, 73 (2005).

[47] J. J. Kolata *et al.*, Phys. Rev. C **69**, 047601 (2004).

[48] N. V. S. V. Prasad *et al.*, Nucl. Phys. A **603**, 176 (1996).

[49] V. Tripathi *et al.*, Phys. Rev. C **65**, 014614 (2001).

[50] S. Sinha, M. R. Pahlavani, R. Varma, R. K. Choudhury, B. K. Nayak, and A. Saxena, Phys. Rev. C **64**, 024607 (2001).

[51] E. M. Szanto *et al.*, Phys. Rev. C **41**, 2164 (1990).

[52] A. M. Stefanini, M. Trotta, L. Corradi, A. M. Vinodkumar, F. Scarlassara, G. Montagnoli, and S. Beghini, Phys. Rev. C **65**, 034609 (2002).

[53] E. M. Martínez-Quiroz, E. F. Aguilera, J. J. Kolata, and M. Zahar, Phys. Rev. C **63**, 054611 (2001).

[54] A. M. Stefanini *et al.*, Phys. Rev. C **62**, 014601 (2000).

[55] L. T. Baby *et al.*, Phys. Rev. C **62**, 014603 (2000).

[56] O. A. Capurro *et al.*, Phys. Rev. C **65**, 064617 (2002).

[57] P. H. Stelson, H. J. Kim, M. Beckerman, D. Shapira, and R. L. Robinson, Phys. Rev. C **41**, 1584 (1990).

[58] S. Mitsuoka, H. Ikezoe, K. Nishio, K. Tsuruta, S. C. Jeong, and Y. Watanabe, Phys. Rev. Lett. **99**, 182701 (2007).

[59] J. O. Newton, C. R. Morton, M. Dasgupta, J. R. Leigh, J. C. Mein, D. J. Hinde, H. Timmers, and K. Hagino, Phys. Rev. C **64**, 064608 (2001).

[60] C. R. Morton, A. C. Berriman, M. Dasgupta, D. J. Hinde, J. O. Newton, K. Hagino, and I. J. Thompson, Phys. Rev. C **60**, 044608 (1999).

[61] R. L. Neto *et al.*, Nucl. Phys. A **512**, 333 (1990).